

1 Defect engineering of the electrochemical characteristics of carbon 2 nanotube varieties

3 Mark A. Hofer and Prabhakar R. Bandaru^{a)}

4 Department of Mechanical and Aerospace Engineering, Materials Science Program,
5 University of California, San Diego, La Jolla, California 92093-0411, USA

6 (Received 11 November 2009; accepted 29 May 2010; published online xx xx xxxx)

7 The electrochemical behavior of carbon nanotubes (CNTs) containing both *intrinsic* and
8 *extrinsically introduced* defects has been investigated through the study of bamboo and hollow
9 multiwalled CNT morphologies. The controlled addition of argon ions was used for varying the
10 charge and type of extrinsic defects. It was indicated from Raman spectroscopy and voltammetry
11 that the electrocatalytic response of hollow type CNTs could be tailored more significantly,
12 compared to bamboo type CNTs which have innately high reactive site densities and are less
13 amenable to modification. An in-plane correlation length parameter was used to correlate the
14 average defect density as a function of argon ion irradiation. The work has implications in the design
15 of nanotube based chemical sensors, facilitated through the introduction of suitable reactive sites.

16 © 2010 American Institute of Physics. [doi:10.1063/1.3457227]

17

18 I. INTRODUCTION

19 The postulated fast electron transfer kinetics,¹ related to
20 the large surface area/volume ratios, of carbon nanotubes
21 (CNTs) could be useful for the development of increased
22 sensitivity electrode materials, electrochemical sensors, su-
23 percapacitors, etc.²⁻⁴ In this context, it has been pointed out
24 that the electrocatalytic behavior along the length of the
25 CNTs would be similar to the basal planes of graphite while
26 the ends would correspond to the edge planes.^{5,6} The latter
27 corresponds to a large defect density, which could be profit-
28 ably used for the enhanced sensitivity. In this study, we in-
29 vestigate the influence of both intrinsic and extrinsic defects
30 through a study of multiwalled, hollow-core CNTs (HCNTs)
31 and bamboo-type CNTs (BCNTs). The HCNTs occur with
32 sidewalls parallel to the nanotube axis—Fig. 1(a), while in
33 the BCNT case, the morphology has periodic graphitic
34 planes, angled away from the tube-axis, forming compart-
35 mentlike structures—Fig. 1(b). The hollow cores in HCNTs
36 arise from the catalyst particle passivation at the center,
37 while the prevention of passivation through using, e.g., NH₃,
38 gives rise to BCNTs.^{7,8} We show that argon ion exposure
39 could be used to systematically tune the electrochemical be-
40 havior of both types of CNTs, through the introduction of
41 additional defective sites with positive charge.

42 The degree of order in CNTs can be studied with Raman
43 spectroscopy through the linear stretching of *sp*² bonds (*E*_{2g}
44 mode), and is manifested through the intensity of the G-peak
45 (frequency ~1580 cm⁻¹). Noncollinear stretches due to de-
46 fects, disorder, or the formation of adsorbates are evidenced
47 through the D-peak,⁹⁻¹² at ~1350 cm⁻¹ in the Raman spec-
48 tra. Additionally, second order harmonic peaks in the range
49 of 2500–3300 cm⁻¹ (e.g., D⁽²⁾/G' ~2700 cm⁻¹, (D+G)
50 ~2930 cm⁻¹) are more sensitive to structural changes in the
51 CNTs (Ref. 10) and were also considered. The in-plane cor-
52 relation length (*L*_a)—the size scale over which the CNT can

be considered defect free, was used as a metric to quantify **53**
the degree of structural disorder and was obtained through a **54**
comparison of the D-and G-peak *intensity* ratio. For ex- **55**
ample, *L*_a is defined by the Tuinstra–Koenig relationship, **56**
*L*_a(nm)=4.4/R where R=(*I*_D/*I*_G)_L. The peak widths [full **57**
width at half maximum (FWHM)] of the G-peaks (i.e., Δ*ω*_G) **58**
and D-peaks (i.e., Δ*ω*_D) are related to the spread of the en- **59**
ergy distribution and were also considered. **60**

Structural modification, through defects, could influence **61**
the predicted performance of CNTs for electrodes and was **62**
investigated through cyclic voltammetry (CV). For example, **63**
in a reversible one-electron transfer from the electrode to the **64**
redox couple [i.e., in Fe(CN)₆³⁻+e⁻↔Fe(CN)₆⁴⁻] the cathodic **65**
peak current density (*i*_{pc}) is equal in magnitude to the anodic **66**
peak current density (*i*_{pa}). Nonideal electrode behavior, **67**
linked to irreversible electron transfer/adsorption processes¹⁵ **68**
would be manifested through (i) a larger/smaller anode- **69**
cathode peak separation (Δ*E*_p=*E*_{pa}-*E*_{pc}) compared to **70**
mV (for a one-electron redox reaction, as above), and/or (ii) **71**
deviations in the |*i*_{pc}/*i*_{pa}| ratio. Changes in the double-layer **72**
capacitance (*C*_{dl}), which arises due to charge separation **73**

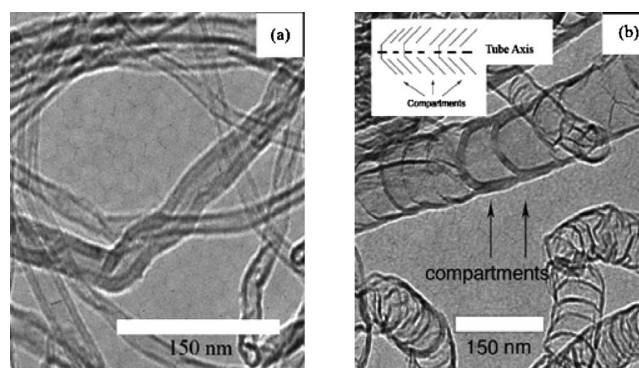


FIG. 1. Transmission electron microscopy images of CNTs of the (a) hollow (HCNT) and (b) bamboo (BCNT) morphology CNTs. The inset of (b) shows the orientation of the graphitic planes.

^{a)}Electronic mail: pbandaru@ucsd.edu.

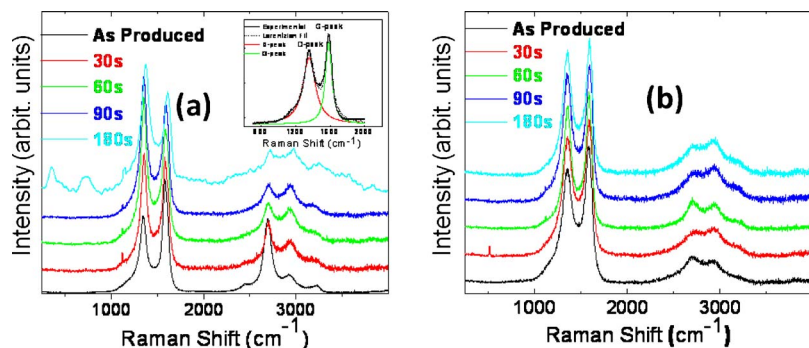


FIG. 2. (Color online) The Raman spectra for the as-produced and Ar exposed (a) BCNTs and (b) HCNTs, irradiated with argon for 30, 60, 90, and 180 s. The inset, in (a) illustrates Lorentzian peak fitting procedures for the D ($\sim 1350 \text{ cm}^{-1}$) and G-peaks ($\sim 1580 \text{ cm}^{-1}$).

74 across the electrode/electrolyte interface, could also indicate
75 changes in the charge density along the CNT.²

76 II. EXPERIMENTAL PROCEDURES

77 Both the hollow core (HCNTs, length $100 \pm 5 \text{ }\mu\text{m}$, di-
78 ameter $17 \pm 3 \text{ nm}$) and bamboo (BCNTs, length $20 \pm 2 \text{ }\mu\text{m}$,
79 diameter $25 \pm 5 \text{ nm}$) CNT morphologies were grown via
80 thermal chemical vapor deposition on n-type Si substrates,
81 using 5 nm thickness of Fe catalyst—deposited through
82 electron-beam evaporation. The HCNTs were grown with a
83 feed gas mixture composed of acetylene [5 SCCM (SCCM
84 denotes cubic centimeter per minute at STP) for 1 min] and
85 200 SCCM argon at $615 \text{ }^\circ\text{C}$. The BCNTs were grown¹⁶ with
86 feed gas composed of 100 SCCM of benzene, 500 SCCM
87 argon, and 200 SCCM ammonia at $850 \text{ }^\circ\text{C}$. Subsequently,
88 for the purpose of introducing a controlled number of de-
89 fects, the CNT samples were subject to argon irradiation in a
90 reactive ion chamber. The influence of a large number of
91 parameters, such as flow rate, irradiation time, power, and
92 ambient pressure were probed. In this paper, a representative
93 study is presented, where an argon flow rate $\sim 10 \text{ SCCM}$,
94 pressure $\sim 30 \text{ mT}$, and power of 100 W was used with time
95 scales in the range of 30–180 s.

96 Raman Spectroscopy (at 514.5 nm, 1.49 mW, with 90 s
97 acquisition time) was then used for quantifying the degree of
98 structural order and charge transfer characteristics,^{11,16,17} in
99 the untreated and argon irradiated samples. The electro-
100 chemical properties of the CNTs were subsequently investi-
101 gated by placing them as working electrodes in CV experi-
102 ments using a PCI4–300 potentiostat from Gamry
103 Instruments Inc. A standard three electrode setup in a 1 M
104 KCl supporting electrolyte solution containing various con-
105 centrations (1–10 mM) of $\text{K}_3\text{Fe}(\text{CN})_6$, was employed with a
106 (i) HCNT/BCNT working electrode, (ii) platinum wire
107 counter electrode, and a (iii) saturated calomel reference

electrode. We eliminated the possibility of hexacyanoferrate
complex adsorbate formation on the electrodes¹⁸ which
could affect electrochemical kinetics, through the choice of
the voltage scan range, of $(-0.4)\text{--}0.8 \text{ V}$, and also through
using freshly prepared ($<2 \text{ h}$ old) solutions.

III. RESULTS AND DISCUSSION

A. Probing the characteristics of irradiated HCNTs and BCNTs through Raman spectroscopy

As the CNTs are exposed to irradiation, the structural
changes were represented by the changes in the first and
second order G- and D-peak intensities (Fig. 2). Lorentzian
fitting functions, for the intensity (I) of the form, I
 $= I_p(\Delta\omega)^2 / 4(f - f_c)^2 + (\Delta\omega)^2$ were used^{12,17,19} for extracting
the peak position (f_c , in per centimeter), the peak height (I_p
in counts), and $\Delta\omega$ (per centimeter). The results for HCNTs
and BCNTs are presented in Tables I and II, respectively.

It was observed from the tables that even in the as-
prepared form, the D-peak position for HCNTs (1347 cm^{-1})
was downshifted $\sim 10 \text{ cm}^{-1}$, compared to the BCNTs
($\sim 1357 \text{ cm}^{-1}$) while the position of the G-peak
($\sim 1585 \text{ cm}^{-1}$) was similar. It was then surmised that the
increased energy of the D-peak in BCNTs was probably due
to the smaller equivalent crystallite sizes,¹⁴ implicit in the
bamboo morphology. Other manifestations of the greater dis-
order were seen through the larger G-peak width ($\sim 82 \text{ cm}^{-1}$
for the BCNTs versus $\sim 70 \text{ cm}^{-1}$ for the HCNTs) along with
a smaller L_a ($\sim 6.0 \text{ nm}$ for the BCNTs versus 6.9 nm for the
HCNTs).

With increasing argon exposure, the following was ob-
served:

- (a) a frequency upshift, along with larger disorder (repre-
sented through an increased $\Delta\omega_G$), of the G-peak. The
disorder was relatively more for the HCNTs (increased

TABLE I. First order characteristics of HCNTs (in Raman spectroscopy), subject to increasing argon irradiation.

Ar irradiation time (s)	G-peak (cm^{-1})	D-peak (cm^{-1})	$(I_D/I_G)_L$	$\Delta\omega_G$ (cm^{-1})	$\Delta\omega_D$ (cm^{-1})	L_a (nm)
0	1586.4 ± 2.1	1347.0 ± 0.7	0.64 ± 0.02	70.0 ± 1.3	116.4 ± 7.5	6.9 ± 0.2
30	1586.0 ± 1.2	1353.0 ± 1.0	0.98 ± 0.08	89.5 ± 3.6	101.9 ± 2.0	4.5 ± 0.4
60	1587.4 ± 1.4	1353.0 ± 1.0	1.10 ± 0.03	89.2 ± 7.4	95.6 ± 7.2	4.0 ± 0.1
90	1588.2 ± 0.5	1353.6 ± 1.2	1.12 ± 0.04	89.3 ± 2.1	99.5 ± 0.5	3.9 ± 0.1
180	1590.2 ± 1.6	1353.8 ± 1.4	1.14 ± 0.07	89.5 ± 5.0	104.8 ± 8.0	3.9 ± 0.2

TABLE II. First order characteristics of BCNTs (in Raman spectroscopy), subject to increasing argon irradiation.

Ar irradiation time (s)	G-peak (cm ⁻¹)	D-peak (cm ⁻¹)	(I _D /I _G) _L	Δω _G (cm ⁻¹)	Δω _D (cm ⁻¹)	L _a (nm)
0	1584.6 ± 1.7	1356.7 ± 2.5	0.73 ± 0.05	82.1 ± 11.8	143.5 ± 41.6	6.0 ± 0.4
30	1587.8 ± 1.1	1359.4 ± 0.9	0.83 ± 0.01	92.6 ± 0.4	155.0 ± 3.9	5.3 ± 0.1
60	1588.0 ± 0.2	1358.0 ± 0.2	0.87 ± 0.03	85.7 ± 8.1	130.1 ± 27.7	5.1 ± 0.2
90	1589.4 ± 2.0	1356.6 ± 1.1	0.88 ± 0.04	90.2 ± 6.8	140.4 ± 17.6	5.0 ± 0.2
180	1591.3 ± 0.7	1356.8 ± 0.7	0.90 ± 0.00	90.9 ± 1.9	131.2 ± 2.8	4.9 ± 0.0

141 from ~70 to ~90 cm⁻¹) compared to the BCNTs (in-
142 creased from ~82 to ~91 cm⁻¹).

143 (b) After initial exposure (i.e., argon for 30 s), the D-peak
144 position and width was relatively unchanged for the
145 HCNT, while it was similarly constant for the BCNTs.
146 (c) A larger increase in the intensity ratio, (I_D/I_G)_L, for the
147 HCNTs compared to the BCNTs was also seen—Fig. 3.

148 (a) suggests that argon ions are being intercalated into
149 the graphene planes forming acceptorlike defects. The higher
150 G-peak frequencies, along with an increase in Δω_G, could be
151 ascribed to a contraction of the intraplanar bond lengths,
152 spanning a distribution of energies. While the G-peak and
153 Δω_G for both HCNTs and BCNTs approach similar values
154 with increased argon exposure (see Tables I and II), indicat-
155 ing a preponderance of defects, the former seem to be more
156 amenable to defect introduction. While argon irradiation
157 does appear to modulate the BCNT characteristics, the intrin-
158 sic defects—due to their morphology as depicted in Fig.
159 1(b), appear to dominate, as also indicated by the constancy
160 of the D-peak from (b) and Table II.

161 The greater sensitivity of second order Raman peaks to
162 both charge and defects was previously noted,¹⁰ and pre-
163 sented in Tables III and IV for HCNTs and BCNTs, respec-
164 tively. For example, the G' peak (the second harmonic of the
165 D-peak, observable at ~2700 cm⁻¹) could be used to study
166 localized charge transfer²⁰ where a frequency upshift would
167 be indicative of acceptorlike doping. Indeed, from the tables,
168 we observe such an increase for both HCNTs (from ~2694
169 to ~2705 cm⁻¹) and BCNTs (from ~2702 to ~2709 cm⁻¹).
170 The sum harmonic (i.e., D+G) peak also indicated such a
171 frequency upshift, for HCNTs (from ~2927 to ~2939 cm⁻¹)

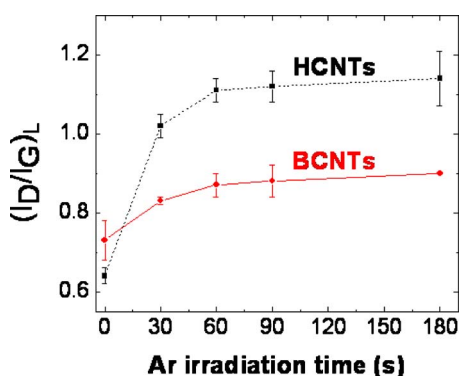


FIG. 3. (Color online) The variation in the line intensity ratio (I_D/I_G)_L for the HCNTs (black) and BCNTs (red), indicates that the former are more amenable to modification.

and BCNTs (from ~2933 to ~2939 cm⁻¹) which could fol-
low from the first order G-peak dependence (Tables I and II).
For the G' peak, the FWHM of the untreated BCNTs, (i.e.,
Δω_{G'} ~ 190 cm⁻¹), was much larger than that of the un-
treated HCNTs, (i.e., Δω_{G'} ~ 111 cm⁻¹), implying greater
localized disorder. However, on exposure to argon, there was
a sudden jump in the linewidth for the BCNT G'-peak, from
~190 to ~293 cm⁻¹, which was relatively unchanged with
further exposure, i.e., through a variation from ~293 to
~300 cm⁻¹, and which suggested a certain and small limit
for argon incorporation. For the HCNTs there was a more
gradual increase in the G'-peak FWHM from ~111 to
~140 cm⁻¹, implying gradual argon insertion. It was also
seen that increasing irradiation decreases the peak intensity,
and implies diminishing second order phonon processes.^{21,22}

In summary, the original defect density seems to dictate
the degree to which the nanotubes could be tailored through
argon exposure. BCNTs with a structural morphology imply-
ing a high intrinsic defect density were less amenable to
subsequent structural and charge modification, compared to
HCNTs.

B. Characterization of HCNTs and BCNTs through CV

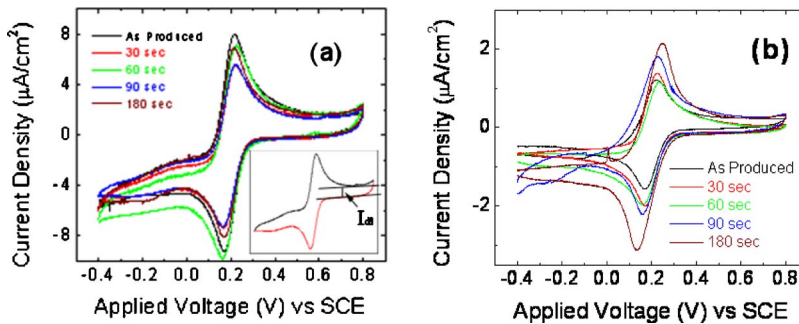
The cyclic voltammograms for the HCNT and BCNT
samples are shown in Fig. 4, and the accrued information
summarized in Tables V and VI, respectively. In the CV
characterization, it was observed that the |i_{pc}/i_{pa}| ratio was
approximately unity for both varieties of nanotubes. How-
ever, an increase in both i_{pc} and i_{pa}, of ~70%, e.g., an in-
crease in i_{pc} from ~1.6 to 2.7 μA/cm², was noted for the
HCNTs (Table V) while the BCNT peak current densities
exhibit a much smaller range of variation of ~25% with
increased argon irradiation time. The increase in the current
density (i_{pa} and i_{pc}) could arise from the availability of ad-
ditional reactive sites/defect density, due to argon irradiation.
A larger peak current density in the BCNTs (Table VI), com-
pared to HCNTs (Table V) could be correlated with a larger
intrinsic defect density in the former. The change in the elec-
trochemical characteristics could be indicated through the
deviation of the ΔE_p (anode-cathode peak potential separa-
tion) from the ideal value of 59 mV, as well. It was seen that
the initial ΔE_p for HCNTs was ~63 mV and for the BCNTs
~46 mV. With increased argon exposure, the ΔE_p exhibited
a much larger variation for the HCNTs (increasing by
~90%, from ~63 to ~118 mV) compared to the BCNTs
(which increases by ~40%, from 46 to 65 mV). ΔE_p values
lower than 59 mV could presumably be due to the adsorption

TABLE III. Second order characteristics of HCNTs (in Raman spectroscopy), subject to increasing argon irradiation.

Ar irradiation time (s)	G'		D+G	
	G' -peak (cm ⁻¹)	$\Delta\omega_{G'}$ (cm ⁻¹)	D+G-peak (cm ⁻¹)	$\Delta\omega_{(D+G)}$ (cm ⁻¹)
0	2693.8 ± 1.1	111.2 ± 19.9	2927.4 ± 4.1	200.3 ± 30.9
30	2698.8 ± 1.2	108.6 ± 4.8	2931.0 ± 4.0	238.8 ± 13.5
60	2702.8 ± 2.4	129.8 ± 19.3	2933.5 ± 2.5	218.0 ± 15.5
90	2703.2 ± 1.6	145.2 ± 5.9	2932.7 ± 1.3	232.4 ± 25.1
180	2704.9 ± 1.4	138.28 ± 11.8	2938.9 ± 6.6	288.6 ± 98.6

TABLE IV. Second order characteristics of BCNTs (in Raman spectroscopy), subject to increasing argon irradiation.

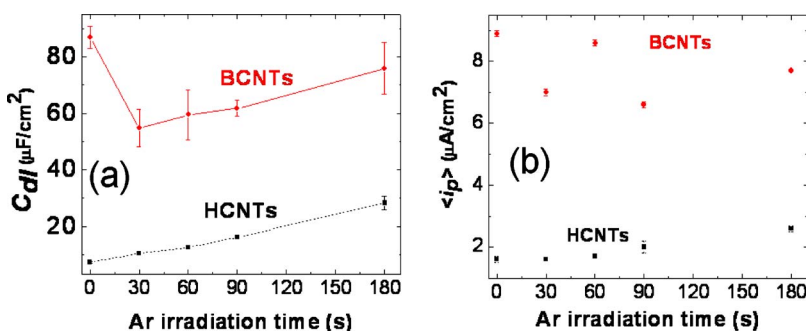
Ar irradiation time (s)	G'		D+G	
	G' -peak (cm ⁻¹)	$\Delta\omega_{G'}$ (cm ⁻¹)	D+G -peak (cm ⁻¹)	$\Delta\omega_{(D+G)}$ (cm ⁻¹)
0	2702.3 ± 4.8	190.0 ± 57.8	2932.7 ± 1.0	223.5 ± 8.9
30	2712.0 ± 1.1	292.7 ± 10.2	2939.1 ± 1.2	254.7 ± 6.2
60	2708.2 ± 3.3	227.2 ± 84.2	2938.5 ± 0.5	230.9 ± 21.1
90	2712.5 ± 5.3	298.9 ± 25.2	2939.8 ± 2.2	228.2 ± 13.4
180	2708.9 ± 3.6	299.8 ± 44.3	2938.6 ± 1.2	229.1 ± 12.4

FIG. 4. (Color online) Cyclic voltammograms for (a) BCNTs and (b) HCNTs as a function of increased argon irradiation. The inset in (a) indicates the procedure through which the double-layer current, I_{dl} , was obtained from a given voltammogram. A scan rate of 20 mV/s with a 3 mM $K_3Fe(CN)_6$ was used.TABLE V. Characteristics of HCNTs obtained through CV, subject to increasing argon irradiation, where $v = 20$ mV/s and $[K_3Fe(CN)_6] = 3$ mM.

Ar irradiation time (s)	i_{pc} (μA/cm ²)	i_{pa} (μA/cm ²)	$ i_{pc}/i_{pa} $	ΔE_p (mV)	C_{dl} (μF/cm ²)	d (nm)
0	1.6 ± 0.3	-1.5 ± 0.0	1.1 ± 0.3	62.5 ± 2.1	7.2 ± 0.4	9.3
30	1.6 ± 0.2	-1.6 ± 0.2	1.0 ± 0.1	51.0 ± 3.0	10.4 ± 0.2	6.7
60	1.7 ± 0.4	-1.7 ± 0.4	1.0 ± 0.1	71.3 ± 8.9	12.5 ± 2.4	5.6
90	2.1 ± 0.3	-1.8 ± 0.3	1.2 ± 0.1	81.0 ± 5.5	16.1 ± 0.5	4.3
180	2.7 ± 0.3	-2.5 ± 0.9	1.1 ± 0.0	118.0 ± 8.4	28.3 ± 2.5	2.5

TABLE VI. Characteristics of BCNTs obtained through CV, subject to increasing argon irradiation, where $v = 20$ mV/s and $[K_3Fe(CN)_6] = 3$ mM.

Ar irradiation time (s)	i_{pc} (μA/cm ²)	i_{pa} (μA/cm ²)	$ i_{pc}/i_{pa} $	ΔE_p (mV)	C_{dl} (μF/cm ²)	d (nm)
0	8.9 ± 0.6	-8.8 ± 1.0	1.0 ± 0.2	45.5 ± 0.7	87.0 ± 4.0	0.9
30	7.1 ± 1.1	-6.9 ± 1.0	1.0 ± 0.1	58.6 ± 5.6	54.8 ± 6.6	1.3
60	8.5 ± 0.3	-8.6 ± 1.0	1.0 ± 0.2	65.7 ± 2.1	59.5 ± 8.8	1.2
90	6.5 ± 0.3	-6.6 ± 0.4	1.1 ± 0.1	59.5 ± 2.1	61.8 ± 2.8	1.1
180	7.7 ± 1.2	-7.7 ± 1.1	1.1 ± 0.3	64.9 ± 1.0	75.9 ± 9.2	1.0

FIG. 5. (Color online) The variation in the (a) double-layer capacitance, C_{dl} and (b) the averaged peak current density, $\langle i_p \rangle$, with argon irradiation time for the HCNTs (black) and BCNTs (red).

of electroactive species onto the CNT electrode,¹⁵ i.e., as $\Delta E_p=0$ mV for adsorbed species (if the oxidized and reduced forms adsorb with the same affinity),²³ a contribution from both adsorbates and species in solution would lead to values intermediate between 0 and 59 mV.

Consequently, both argon irradiated HCNTs and BCNTs indicate quasireversible electron transfer kinetics, with greater influence manifested in the HCNTs.^{15,20} Such diminished kinetics could arise from an increased density of species surrounding the CNTs and may be brought about by the enhanced number of defects. The ΔE_p may also increase due to the increased activation energy, intrinsic to the defective sites induced by irradiation, for the occurrence of electrochemical reactions. An additional metric could then be the value of the double-layer capacitance (C_{dl}) which denotes the change in the CNT electrode characteristics as a function of argon irradiation. In this case, an increased defect density could presumably result in larger capacitance values. We calculated C_{dl} from the double-layer current I_{dl} ($=v C_{dl}$), at a given scan rate, v (in millivolt per second). I_{dl} was determined from the cyclic voltammogram using procedures outlined in Bard and Faulkner,¹⁵ and indicated in the inset to Fig. 4(a). We used a simple approximation, using the Helmholtz model,²³ for $C_{dl}(=\epsilon\epsilon_0A/d)$, modeling the capacitance as due to a double layer of thickness, d , with A as the electrode area, ϵ the dielectric permittivity of the surrounding solution (~ 80), and ϵ_0 being the permittivity of free space ($=8.854 \times 10^{-12}$ C²/Nm²). It is noted that as the volume ratio of KCl to water is $\sim 1:24$, an estimate of ~ 80 for ϵ is reasonable. Additional considerations,²⁴ incorporating polarization and hydration effects also yield a variability of ϵ at most $\sim 10\%$. This in turn implies an equivalent error in the estimation of the C_{dl} and is close to the experimental error, as indicated in Tables V and VI.

Generally, the Helmholtz model is quite simplistic compared to other models such as the Stern model or the more advanced chemical models.²³ However, the net capacitance is determined by the parallel combination of the fixed double layer, diffuse layer, solvent layer, etc. As we operate at values of applied potential larger than that corresponding to the point of zero charge, it could be a reasonable estimate to consider the capacitance due to the fixed double layer alone, as is assumed in the model. While we have observed a dependence of the capacitance on the concentration (which is again not considered in the Helmholtz model), in this paper we analyze results at a particular value of the concentration, i.e., 3 mM (as in Tables V and VI) for which our modeling might be adequate.

The area of the CNT electrode was approximated to be ~ 110 m²/g and ~ 75 m²/g for HCNTs and BCNTs, respectively, through considering the total surface area of the nanotubes,²⁵ treating each CNT as an individual electrode. Generally, in the use of CNTs as electrodes, one can consider two possibilities, i.e., corresponding to the cases where (1) each CNT acts as an independent electrode or (2) the individual diffusion layers of each CNT overlap resulting in a macroelectrodelike behavior. In case (1), the effective area could be estimated by considering the CNTs to be cylindrical with an average surface area of $2\pi rh$ and multiplying by the

total number of CNTs on the Si substrate (estimated from an average spacing between the grown CNTs and the length and width of the Si substrate). This results in a total electrode area of the order of 10 cm². In case (2), the projected area of the substrate is considered and yields a total area of the order of 0.05 cm² (say, corresponding to a 7×7 mm² substrate).

When the value of the d , corresponding to cases (1) and (2) is estimated from the C_{dl} , for the latter case we seem to obtain unrealistic d values of the order of ~ 0.006 nm! Even if it is assumed that the ions are intimately adsorbed to the CNT surface, the ΔE_p should be ~ 0 , which was not seen. The results of the computed C_{dl} for HCNTs and BCNTs subject to argon exposure are indicated in Tables V and VI, respectively, and are plotted in Fig. 5(a). It was seen that, C_{dl} of the HCNTs increases ($\sim 300\%$) with increased argon irradiation, along with a concomitant increase in the magnitude of E_{pa} , E_{pc} , and hence ΔE_p , while the C_{dl} of the BCNTs remains relatively constant. Contrary to HCNTs, intrinsic defects and morphology seem to dominate over the influence of those defects generated through argon exposure in BCNTs.

IV. CONCLUSIONS

We have shown that exposure to argon irradiation, through the controlled incorporation of defects, can influence the charge state of both *bamboo* and *hollow* variety CNT morphologies. Raman spectroscopy analysis, through the peak shifts and broadening, indicated nanotube charging and passivation. It is plausible that argon, through intercalation in the CNTs, abstracts electrons creating acceptor like defects. It was also concluded that the initial structural state could limit the relative amount of charge and defects that could be introduced. Consequently, BCNTs seem to be inherently better, compared to HCNTs, for electrodes in electrochemical processes due to larger intrinsic defect density. However, HCNTs allow for a greater degree of tunability and a range of electron transfer kinetics, made possible through argon irradiation. While the peak potential difference, ΔE_p , was seen to increase for both BCNTs and HCNTs due to argon exposure, the peak current ratio $|i_{pc}/i_{pa}|$, remained close to unity indicating quasireversible kinetics. Our work contributes to a better understanding of defects in CNTs and could be applied for tuning the electrochemical properties of CNT based electrodes, e.g., in chemical sensors and capacitors.

ACKNOWLEDGMENTS

We gratefully acknowledge support from the National Science Foundation (Grant No. ECS-05-08514) and the Office of Naval Research (Award No. N00014-06-1-0234). We thank Professor Frank Talke's group at the Center for Magnetic Recording Research (CMRR) at UC, San Diego for help with the Raman spectroscopy.

¹J. M. Nugent, K. S. V. Santhanam, A. Rubio, and P. M. Ajayan, *Nano Lett.* **1**, 87 (2001).

²M. Hoefler and P. R. Bandaru, *Appl. Phys. Lett.* **95**, 183108 (2009).

³R. H. Baughman, A. A. Zakhidov, and W. A. de Heer, *Science* **297**, 787 (2002).

⁴Q. Zhao, Z. Gan, and Q. Zhuang, *Electroanalysis* **14**, 1609 (2002).

⁵C. E. Banks, R. R. Moore, T. J. Davies, and R. G. Compton, *Chem. Commun. (Cambridge)* **2004**, 1804.

- AQ:** **334** ⁶C. E. Banks, T. J. Davies, G. G. Wildgoose, and R. G. Compton, *Chem. Commun. (Cambridge)* **2005**, 829 (2005). **351**
- #2** **335** ⁷F. Ding, K. Bolton, and A. Rosen, *J. Electron. Mater.* **35**, 207 (2006). **352**
- 336** ⁸C. H. Lin, H. L. Chang, C. M. Hsu, A. Y. Lo, and C. T. Kuo, *Diamond Relat. Mater.* **12**, 1851 (2003). **353**
- 337** ⁹T. C. Chieu, M. S. Dresselhaus, and M. Endo, *Phys. Rev. B* **26**, 5867 (1982). **354**
- 338** ¹⁰M. S. Dresselhaus, G. Dresselhaus, A. Jorio, A. G. Souza Filho, and R. Saito, *Carbon* **40**, 2043 (2002). **355**
- 339** ¹¹M. S. Dresselhaus, G. Dresselhaus, M. A. Pimenta, and P. C. Eklund, in *Analytical Applications of Raman Spectroscopy*, edited by M. J. Pelletier (Blackwell Science, Malden, 1999), pp. 367–434. **357**
- AQ:** **341** ¹²B. S. Elman, M. S. Dresselhaus, G. Dresselhaus, E. W. Maby, and H. Mazurek, *Phys. Rev. B* **24**, 1027 (1981). **358**
- #3** **342** ¹³D. S. Knight and W. B. White, *J. Mater. Res.* **4**, 385 (1989). **359**
- 343** ¹⁴F. Tuinstra and J. L. Koenig, *J. Chem. Phys.* **53**, 1126 (1970). **360**
- 344** ¹⁵A. J. Bard and L. R. Faulkner, *Electrochemical Methods: Fundamentals and Applications*, 2nd ed. (Wiley, New York, 2001). **361**
- 345** ¹⁶B. S. Elman, M. S. Dresselhaus, M. Shayegan, H. Mazurek, and G. Dresselhaus, *Phys. Rev. B* **25**, 4142 (1982). **362**
- 346** ¹⁷J. Robertson, *Mater. Sci. Eng. R.* **37**, 129 (2002). **363**
- 347** ¹⁸C. M. Pharr and P. R. Griffiths, *Anal. Chem.* **69**, 4673 (1997). **364**
- 348** ¹⁹E. F. Antunes, A. O. Lobo, E. J. Corat, V. J. Trava-Airoldi, A. A. Martin, and C. Verissimo, *Carbon* **44**, 2202 (2006). **365**
- 349** ²⁰K. McGuire, N. Gothard, P. L. Gai, M. S. Dresselhaus, G. U. Sumanasekera, and A. M. Rao, *Carbon* **43**, 219 (2005). **366**
- 350** ²¹A. C. Ferrari and J. Robertson, *Phys. Rev. B* **61**, 14095 (2000). **367**
- ²²P. C. Eklund, J. M. Holden, and R. A. Jishi, *Carbon* **33**, 959 (1995). **361**
- ²³C. M. A. Brett and A. M. O. Brett, *Electrochemistry: Principles, Methods, and Applications* (Oxford University Press, Oxford, 1993). **362**
- ²⁴K. Nörtemann, J. Hilland, and U. Kaatzke, *J. Phys. Chem. A* **101**, 6864 (1997). **363**
- ²⁵A. Peigney, C. Laurent, E. Flahaut, R. R. Basca, and A. Rousset, *Carbon* **39**, 507 (2001). **364**

AUTHOR QUERIES — 095013JAP

- #1 Au: Please verify changes made in author names and volume no. in Ref. 5.
- #2 Au: Please verify changes made in volume no. in Ref. 6.
- #3 Au: Please verify the changes made in the first page no. in Ref. 9.
- #4 Au: Although a caption makes reference to color online, figures will appear black and white in print. Please make sure that the caption makes sense to print reader.